 AIAA 2013-2031

Interior Analysis of Impulse Noise from Weapons in a Perspective on Damage Risk Using the Alternative Image Theory

Byunghak Kong[1]
Seoul National University, Seoul 151-742, Korea

Sung-Soo Jung[2]
Korea Research Institute of Standards and Science, Daejeon 305-340, Korea

Eunkuk Son[3] and Soogab Lee[4]
Seoul National University, Seoul 151-742, Korea

and

Kee Hyeok Song[5]
Agency for Defense Development, Daejeon 305-152, Korea

Blast waves generated from the muzzles of various weapons might have significant effects on the operators' body, such as hearing loss. If the weapon is operated in a room, these effects are recognized as being more severe. MIL-STD-1474D, a damage risk criterion that considers the peak sound pressure level and B-duration time and is recommended by the US Department of Defense, is widely used because of its simplicity. This study introduces a numerical model of damage risk assessment based on the alternative image theory and discrete wavefront method. The alternative theory is a technique for predicting the effect of reflected waves using the image space concept, and the wavefront method is a propagation model based on the blast waveform. Sound pressure distributions inside an enclosed space and signals at specific positions were obtained using the model. Although the estimated results differ slightly from the measured ones, the waves reflected from the enclosing boundaries were effectively captured with good agreement, as expected.

Nomenclature

A	=	magnitude of blast overpressure
α_1	=	coefficient related to half width of Gaussian pulse
B	=	coefficient related to negative phase of blast wave
E, F	=	conservative variables in x-, and y-direction, respectively
ε_1	=	coefficient related to amplituce of Gaussian pulse
η	=	variable related to distance between the source and the receiver
γ	=	specific heat ratio
J_0	=	Bessel function of order zero
k	=	wavenumber
p	=	acoustic pressure disturbance (with respect to mean flow pressure, p_0)
Q	=	spherical wave reflection coefficient

[1] Ph.D. Student, School of Mechanical and Aerospace Engineering, #311-105, 1 Gwanak-ro, Gwanak-gu.
[2] Principal Research Scientist, Division of Physical Metrology, 267 Gajeong-ro, Yuseong-gu.
[3] Ph.D. Student, School of Mechanical and Aerospace Engineering, #311-105, 1 Gwanak-ro, Gwanak-gu.
[4] Professor, Institute of Advanced Aerospace Technology and School of Mechanical and Aerospace Engineering, #311-105, 1 Gwanak-ro, Gwanak-gu.
[5] Researcher, Advanced Propulsion Technology Center, 106 Bugyuseong-daero 488 beon-gil, Yuseong-gu.

R = distance between source and receiver related to specific image space
ρ = density disturbance (with respect to mean flow density, ρ_0)
t = time
τ = duration time (A-type)
U = conservative variables related to temporal derivative
u, v = velocity disturbances in x-, and y-direction (with respect to mean flow velocities, u_0 and v_0)
w = indices for each boundaries in two-dimensional rectangular space (subscribed with *1*, *2*, *3*, *4*)
x, y = position of receiver inside the space in Cartesian coordinate

I. Introduction

PREVENTING damage to the body of an operator is one of the most significant and difficult challenges in the development of guided weapons for indoor use. For instance, potential damage includes hearing loss and burns due to contact with either a guide or flames[1-3]. In particular, hearing loss is caused by strong blast waves that develop when a firearm is firing. However, they are a great concern indoors because they reverberate within the indoor space instead of diverging into the atmosphere, as they do when outdoors[4]. Hence, the risk that they will damage the human body is assessed by various procedures and is legally restricted according to regulations and legislation[5-14]. The damage risk criteria (DRCs) are classified into three types: waveform parameter-based DRCs, equivalent-energy DRCs, and model-based DRCs[10]. The first type, waveform parameter-based methods, uses waveform parameters obtained from the acoustic pressure signal to assess the risk. MIL-STD-1474D[6], which was established by the United States Department of Defense, is representative of this type. Using MIL-STD-1474D, which is an advanced version of the Committee on Hearing, Bioacoustics, and Biomechanics (CHABA)[5] including a level shift corresponding to the effectiveness of hearing protection[13], the expected number of daily exposures and the type and number of protectors are determined by the peak sound pressure level (SPL) and the B-duration obtained from the measured pressure signal. On the other hand, the second type, equivalent-energy methods, bases the assessment on the entire acoustic energy to which a person is exposed, e.g., the sound exposure level (SEL) and equivalent continuous A-weighted SPL[10-11].

When these methods are implemented in damage risk assessment, the assessment is usually conducted using experimentally measured pressure signals. However, because it is possible to obtain different results for each experiments, the degree of damage risk has been unclear. For many years, the worst case round among all the test rounds and firing conditions was conservatively used to assess the hazard because this is a problem directly related to the human body. However, Patterson recently derived a type of post processing known as the proportional dose method[15-16], which may weaken and extend the conservativeness and range of utilization, respectively. To eventually resolve this problem, though, it is essential to develop a prediction model. Furthermore, the damage risk can be effectively evaluated using the prediction model considering many parameters related to the operating conditions, such as directional angle, the dimensions of the space, and the enclosing materials.

This research focuses on developing a fundamental prediction model that can simulate the propagation of blast waves generated during propellant combustion when a guided weapon is fired in an interior space and that can be applied to estimate the peak SPL distribution, which enables to the assessment of damage risk according to MIL-STD-1474D. In particular, this process might be complete in a sufficiently short time to be portable for use in the battlefield because it adopts an alternative image theory[17] and discrete wavefront method instead of the numerical schemes widely used in computational fluid dynamics and computational aeroacoustics. Section 2 describes the image space and folding method concepts, which are the principles of the alternative theory and describe the effect of reflected waves, and the discrete wavefront method, which is used as an independent propagation model. In section 3, numerical analysis is performed using the prediction model, and the accuracy, validity, and critical issues are investigated by comparing the numerical and measured results.

II. Methodologies

A. Alternative Image Theory

1. Image Space Concept

In the original image theory, the sound field resulting from a point source above the ground is interpreted as a superposition of a direct wave from the real source and a reflected wave from the image source. This can be applied identically to an interior problem, in principle, but the number of terms indicates the effect of reflected waves increases because there are several boundaries, unlike the situation outdoors. For instance, the acoustic pressure distribution, $p(x, y)$, over a two-dimensional rectangular space enclosed by four boundaries is represented as follows:

$$p(x,y)=\frac{e^{-ikR_0}}{4\pi R_0}+\left(Q_{w_1}\frac{e^{-ikR_{w_1}}}{4\pi R_{w_1}}+Q_{w_2}\frac{e^{-ikR_{w_2}}}{4\pi R_{w_2}}+Q_{w_3}\frac{e^{-ikR_{w_3}}}{4\pi R_{w_3}}+Q_{w_4}\frac{e^{-ikR_{w_4}}}{4\pi R_{w_4}}\right)$$
$$+\left(Q_{w_1}Q_{w_2}\frac{e^{-ikR_{w_1,w_2}}}{4\pi R_{w_1,w_2}}+Q_{w_1}Q_{w_3}\frac{e^{-ikR_{w_1,w_3}}}{4\pi R_{w_1,w_3}}+\cdots+Q_{w_3}Q_{w_4}\frac{e^{-ikR_{w_3,w_4}}}{4\pi R_{w_3,w_4}}\right) \quad (1)$$
$$+\left(Q_{w_1}Q_{w_3}Q_{w_1}\frac{e^{-ikR_{w_1,w_3,w_1}}}{4\pi R_{w_1,w_3,w_1}}+\cdots+Q_{w_4}Q_{w_2}Q_{w_1}\frac{e^{-ikR_{w_4,w_2,w_1}}}{4\pi R_{w_4,w_2,w_1}}+\cdots\right)+\cdots.$$

In this equation, Q and R are the spherical wave reflection coefficients corresponding to each boundary condition and the distance in the propagation path related to reflection(s) between either the real or the image source, respectively, and the receiver. In contrast to the sound field near the ground, the interior sound field is expressed in a longer equation than that representing the field outdoors because multiple reflections due to adjacent enclosing boundaries should be considered. In particular, if the number of boundaries enclosing the space and the maximum number of reflections increase, the number of terms included in the equation also increases. Consequently, the number of image sources required for prediction also increases.

If the alternative image theory adopting an image space concept is implemented for interior analysis, these difficulties can be resolved. The image space is an extention of the concept of the image receiver, which is the opposite of the image source, and can be determined by a simple procedure. When an interior space, represented by a computational domain, is composed of a finite number of real receivers depending on discretization, as shown in Fig. 1-(a), a set of them can be defined as the original domain, which is called the real space hereafter. Then, the image spaces can be defined according to the relative locations of the real space and reflecting surfaces, considering the number of reflections. In other words, each image space is configured symmetrically with respect to real space on the basis of the geometrical relations between the boundaries being passed, and is uniquely determined by a corresponding set of boundaries, as shown in Fig. 1-(b). In addition, the number of reflecting boundaries, which is the same as the number of reflections, is defined as the order of the corresponding image space.

When the maximum number of reflections required for analysis is determined, the image spaces are configured according to the procedure described above. At this time, they are sequentially arranged from low order to high order; it is also important to note that no reflections occur consecutively from the same boundary. That is, the image spaces are configured in a direction away from the real space.

Implementing the alternative image theory in terms of the image space concept for indoor sound propagation is expected to yield two major advantages. First, because the image space is obtained using both the shape of the real space and the arrangement of the boundaries and is independent of the position of the real source, an algorithm for finding the locations of the image sources is not required. Furthermore, the sound field can be intuitively examined in terms of a single source because the computational domain including both the image and real spaces is a free

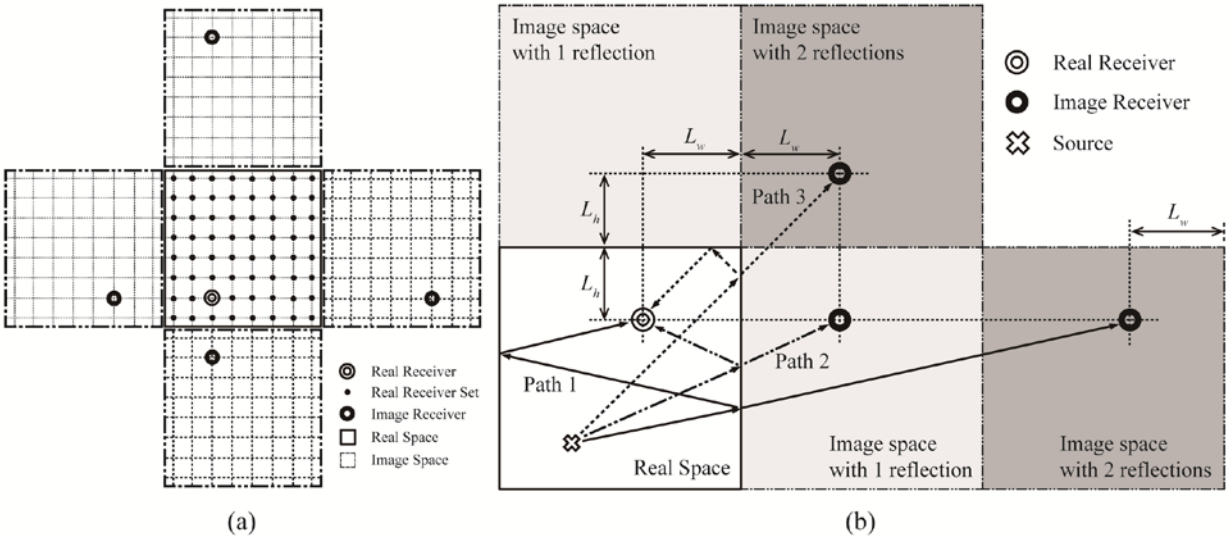

Figure 1. (a) Image space concept and (b) its configuration depending on the order.

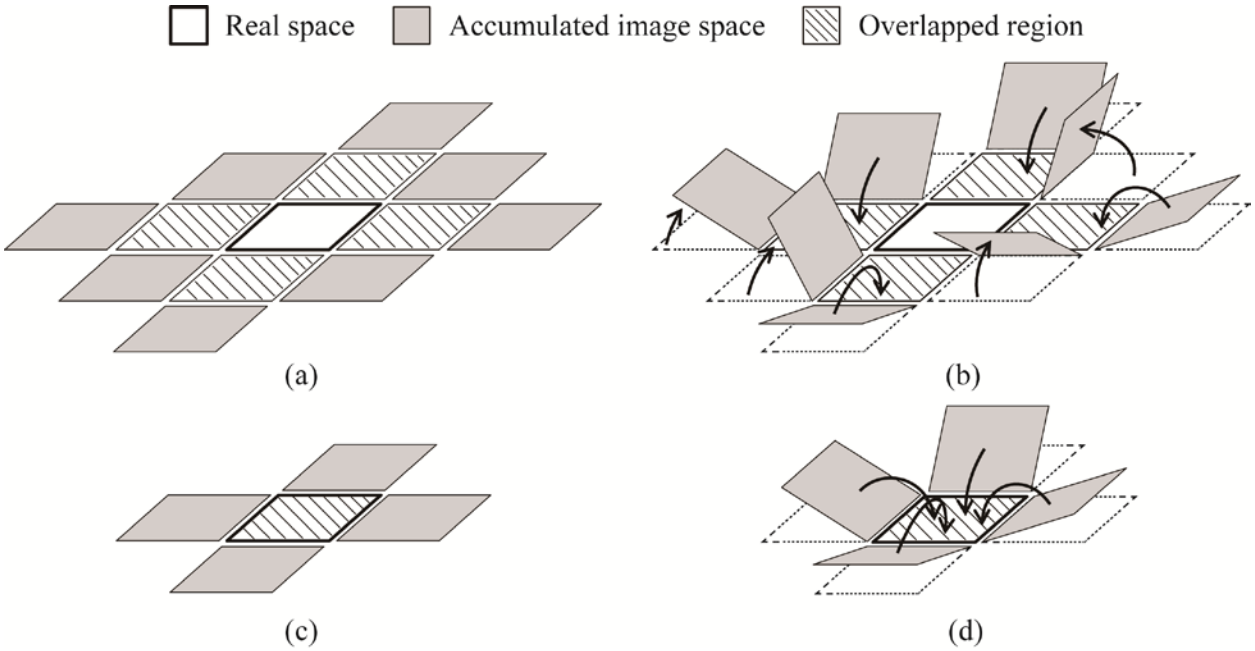

Figure 2. Schematic illustration of the folding method.

space, which means that no boundary condition is needed on the outer boundaries. In this study, only rectangular spaces are considered to avoid a complicated situation in which image spaces overlap one another.

2. Folding Method

The sound field resulting from the reflected waves is formed, and each field is expressed as an independent term in Eq. 1. Therefore, to predict the sound pressure distribution inside the space, it is necessary to aggregate not only the sound fields from the direct wave but also those from the waves reflected into the real space. In this research, this process is called the folding method.

The folding method is performed in the reverse order compared to the configuration of the image space. In other words, whereas the image spaces were generated by inverting either the real space or the lower-order image spaces with respect to their boundaries, the folding method represents the superposition of the sound fields by folding the image spaces into the next-lower-order spaces with respect to their boundaries. This process is illustrated in detail in Fig. 2. The folding sequence is followed by inverting the highest-order image spaces belonging to the computational domain to the next-lower levels. If it is reasonably assumed that the sound field is rarely affected by the order of the boundaries it passes through, the effect of the reflections can be represented by the folding method. Consequently, the sound pressure distribution over the real space can be obtained as shown in Fig. 2-(d).

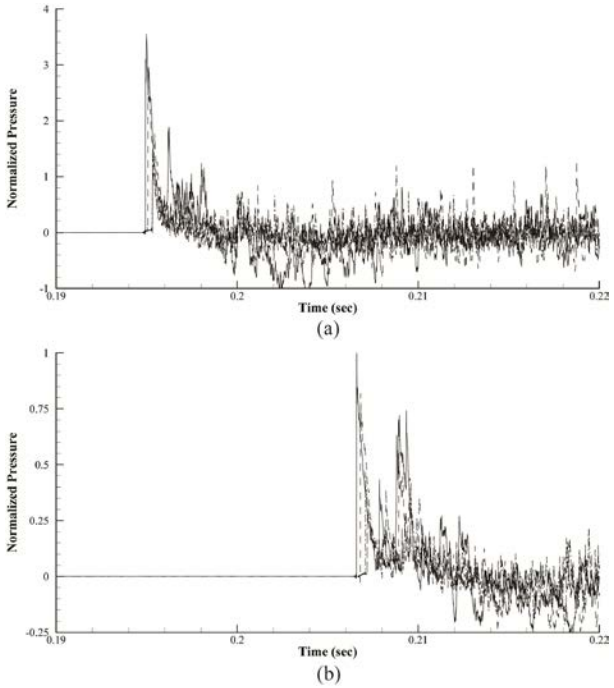

Figure 3. Normalized acoustic pressure signals measured (a) 2 m and (b) 6 m from the source at 25, 40, 55, 70 and 90°.

B. Discrete Wavefront Method

The sound field induced inside the computational domain, including the real and image spaces, can be predicted by various numerical techniques such as computational aeroacoustics, the finite element method, and the boundary element method. Because blast waves

are representative of nonlinear phenomena, high-order numerical schemes are needed to obtain accurate results. Consequently, these techniques inevitably require considerable time and are costly. Therefore, they do not satisfy the major objective of this research. Hence, a simple propagation model for blast waves based on previous studies is introduced.

Kinsler et al.[19] defined a blast wave as a spherically expanding shock front that propagates out into the quiescent atmosphere. From a different perspective, it is thought that a blast wave moves away from a source with similar speed in all directions. This can be verified by acoustic pressure signals, as shown in Fig. 3. These are the normalized acoustic pressure signals measured 2 m [Fig. 3-(a)] and 6 m [Fig. 3-(b)] from the source at 25, 40, 55, 70 and 90° relative to the line of combustion jet flow when a missile was launched from a guided weapon. Each of the five blast waves measured at the same distance was captured at almost the same time regardless of the directional position. Therefore, it is reasonable to conclude that blast waves propagate outward with nearly the same speed and maintain their spherical shapes. If the effect of fluctuations generated by combustion jet flow on the peak SPL distribution can be ignored, the blast wave might be simplified according to the following waveform equation[19] modified from the Friedlander equation[20].

$$p(t) = A\left[1-\left(\frac{t}{\tau}\right)\right]e^{-B(t/\tau)} \tag{2}$$

In Eq. 2, τ is the A-duration time[8], and A and B indicate the magnitude of the blast overpressure and a coefficient related to the characteristic of negative phase duration, respectively. Figure 4 shows the simplified blast wave according to Kinsler model[19] described in Eq. 2, with A = 10,400, B = 0.8, and τ = 0.001, compared with the measured acoustic pressure signal. According to Fig. 4, although the section where the first and principal peak is formed was coincides with the measured signal, the other part, especially negative phase duration, did not. This discrepancy results essentially from the difference in the interior ballistics mechanism between typical rifles and the guided weapon. Nevertheless, because it is reasonable to assume that the peak SPL is rarely affected by the negative phase, the blast waveform depicted in Fig. 4 was used in this study.

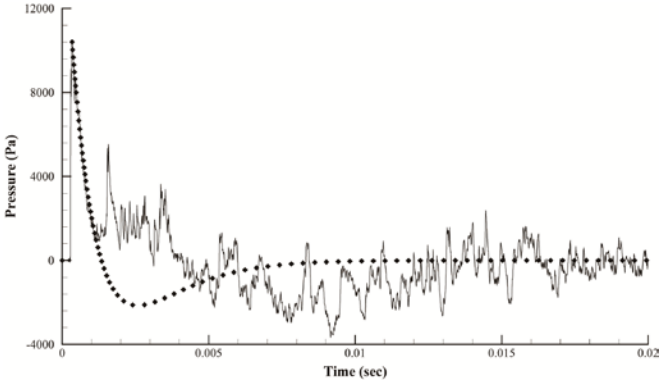

Figure 4. Comparison of measured signal (solid line) and designed signal by Kinsler model[19] (symbols).

Next, the blast wave zone corresponding to the blast waveform can be established and is divided into a finite number of discrete wavefronts at regular intervals, as shown in Fig. 4-(a). The wavefront is described by two different definitions[21]. The first definition is a surface of

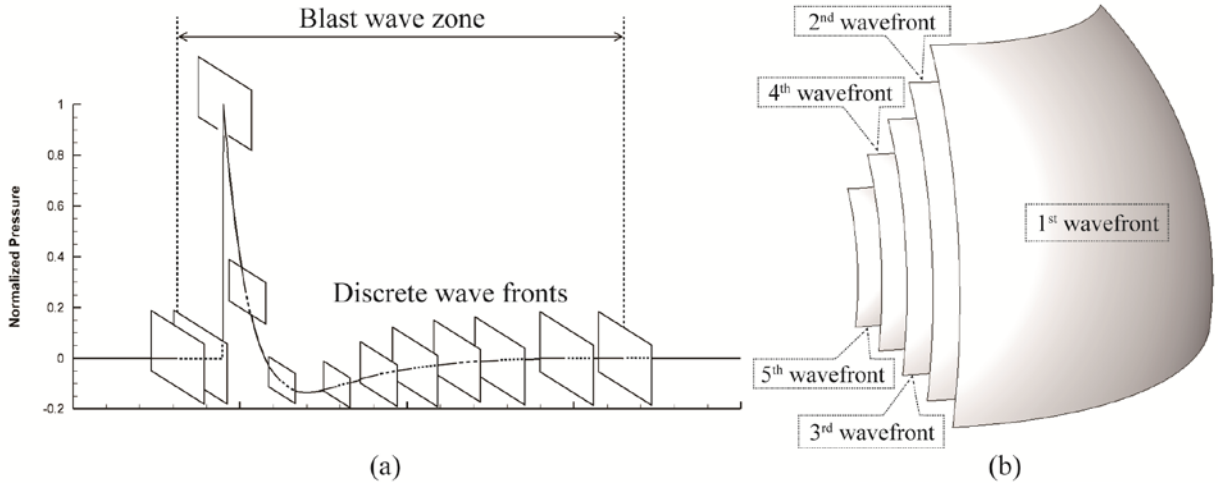

Figure 5. Descriptions of blast wave zone and discrete wave fronts in (a) one- and (b) three-dimensional space.

constant phase in a single-frequency progressive wave field, and the other indicates a propagating surface of discontinuity across which an acoustic variable (e.g., the pressure) changes by a vanishingly small amount. This study adopts the second definition. Theoretically, a set of discrete wavefronts for the waveform in Fig. 4 can be obtained, as shown in Fig. 5-(a). If a three-dimensional space is considered, the spherical wavefronts shown in Fig. 5-(b) might be configured.

These steps are required to interpret blast wave propagation into a medium as the forward movement of each wavefront in the propagation direction. Under these circumstances, the speed and direction of an arbitrary point on the wavefronts are determined in terms of the mean flow velocity and speed of sound at that position according to Huygen's principle[22]. In this study, it was assumed that information about the relative position in the blast wave zone and the acoustic pressure were assigned to each wave front, and they advanced with the same speed and maintained the initial intervals. For example, when a blast wave in three-dimensional space is considered, the movement of wavefronts described as spherical surfaces can be presented as expansion of concentric spheres. Simultaneously, as the wavefronts expands, the acoustic pressure on their surfaces is attenuated because of geometrical divergence.

III. Results and Discussions

A. Validation for the Alternative Image Theory

To validate the alternative image theory, numerical analyses in two-dimensional space were performed, and the results were compared to those using another numerical scheme in which an analytical solution is used as a wave propagation technique instead of the additional scheme.

Figure 6-(a) shows a rectangular space divided into a 150 by 100 mesh. Because the wall boundary condition was applied to the lower boundary, the computational domain can be configured as only a single first-order image space. The boundary was assumed to be a perfectly reflecting surface; consequently, the reflection coefficient was considered to be unity. The simulation used an optimized fourth-order central-difference scheme, the so-called dispersion-relation-preserving (DRP) scheme developed by Tam, and a fourth-order Adams-Bashforth method, which correspond to spatial and temporal differential schemes, respectively. A governing equation, the linearized Euler equation for two-dimensional disturbances used in the analysis and its conservative variables are as follows[23-24]:

$$\frac{\partial U}{\partial t}+\frac{\partial E}{\partial x}+\frac{\partial F}{\partial y}=0\,.$$

$$U=\begin{bmatrix}\rho\\ u\\ v\\ p\end{bmatrix},\ E=\begin{bmatrix}\rho_0 u+\rho u_0\\ u_0 u+p/\rho_0\\ u_0 v\\ u_0 p+\gamma p_0 u\end{bmatrix},\ F=\begin{bmatrix}\rho_0 v\\ 0\\ p/\rho_0\\ \gamma p_0 v\end{bmatrix} \tag{3}$$

Small-amplitude disturbances, including those in density ρ, velocities u and v, and pressure p, which were nondimensionalized by using the proper scale values, are superimposed on a uniform mean flow of ρ_0, u_0, and p_0. In this study, it was assumed that the velocity in the x direction is zero, and the density and pressure are unity. Then, the initial conditions was imposed, and subsequently, numerical analysis was conducted by applying the DRP scheme[23-24]. The initial conditions consist of a Gaussian pulse described as follows:

$$u=v=0,\ \ p=\rho=\varepsilon_1\exp\left[-\alpha_1\left(x^2+y^2\right)\right]$$

In this case, the coefficients ε_1 and α_1, were 0.01 and (ln2)/9, respectively. The analytic solution corresponding to the governing equation, Eq. 3, and the initial conditions is expressed as follows[23-24]:

$$p(x,y,t)=\frac{\varepsilon_1}{2\alpha_1}\int_0^\infty e^{-\xi^2/4\alpha_1}\cos(\xi t)J_0(\xi\eta)\xi d\xi\,. \tag{4}$$

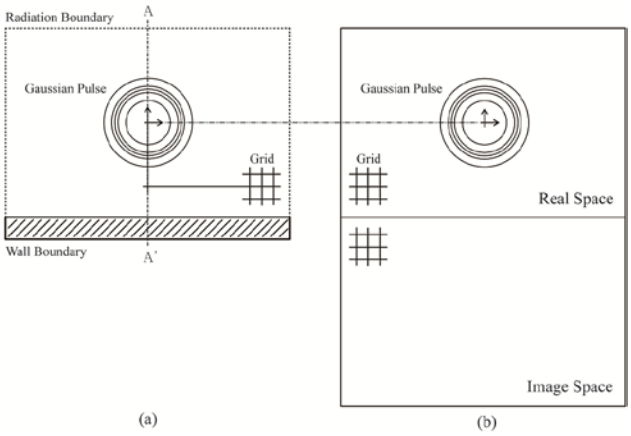

Figure 6. Schematics of (a) the real conditions in two-dimensional space with a wall boundary at the lower side compared with (b) the alternative method.

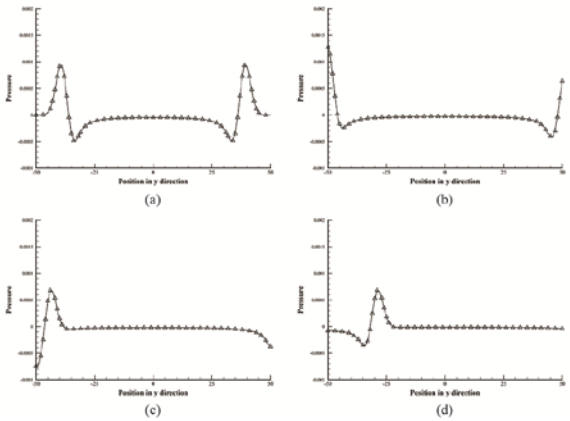

Figure 7. Comparison of the numerical results from the alternative image theory (solid line) and the DRP scheme (triangles) at the normalized times (a) 38, (b) 50, (c) 55, and (d) 70 at the cross-sectional position (A-A′) in Fig. 6-(a).

In Eq. 4, $\eta = (x^2 + y^2)^{1/2}$, and J_0 is the Bessel function of order zero. The acoustic pressure distribution over the entire domain, including the image space, was simulated by applying the analytic solution and those in the image space were inverted into the real space using the folding method. Then, the resulting distribution inside the two-dimensional space, with a single reflecting surface, can be obtained for a specific time.

Figure 7 compares the numerical results from the DRP scheme and the alternative theory. It shows the pressure distributions at the cross-sectional position (A-A′) in Fig. 6-(a). They were captured consecutively at the normalized times 38, 50, 55, and 70 as predicted by the alternative image theory and the DRP scheme. The numerical results obtained by these two methods agreed perfectly. Therefore, we conclude that the alternative theory can be applied to interior analysis including multiple reflections.

B. Interior Analysis

The alternative theory was implemented in an analysis in three-dimensional space, and the results were compared to acoustic pressure signals measured at specific locations during experiments. Figure 8 shows the dimensions of the space, which is 35 m^3 in volume, and the locations of the source and microphones. Although the side walls contained launch and monitoring windows and a rear door, which was open, when the experiments were conducted, it was assumed that the entire boundaries were closed and the reflection coefficient was unity in the analysis. Likewise, the effects of the missile guide and instruments were ignored. Finally, because the maximum number of reflections was set to three, the computational domain was composed of 63 image spaces and the real space.

The discrete wavefront method introduced in section 2 was used as the propagation model. The waveform shown in Fig. 5-(a) was adopted, and a set of spherical wavefronts was developed according to this waveform. They were also used as the initial conditions, which were arranged with respect to a wavefront corresponding to the maximum peak located 0.2 m from the source. Subsequently, the initial directivity pattern was modified according to the angular acoustic overpressure distribution relative to the line of turbulent jet flow estimated by the least square method according to the signals measured during exterior experiments, assuming axisymmetry. It was also assumed that the wavefronts propagated with the same speed, 340 m/s, regardless of their

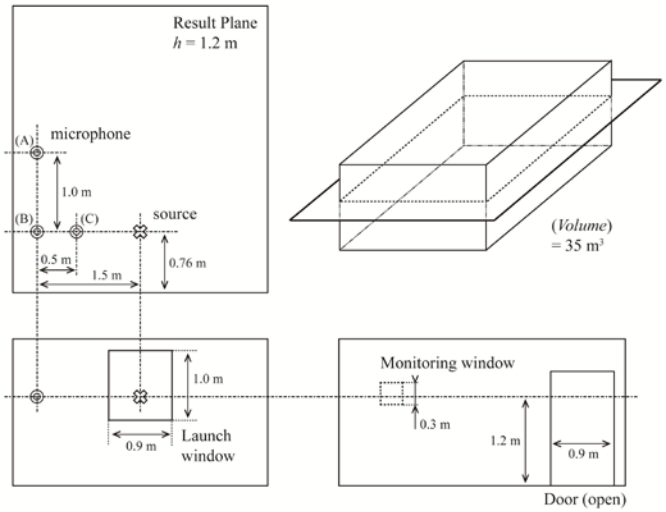

Figure 8. Dimensions of the space and the locations of the source and microphones.

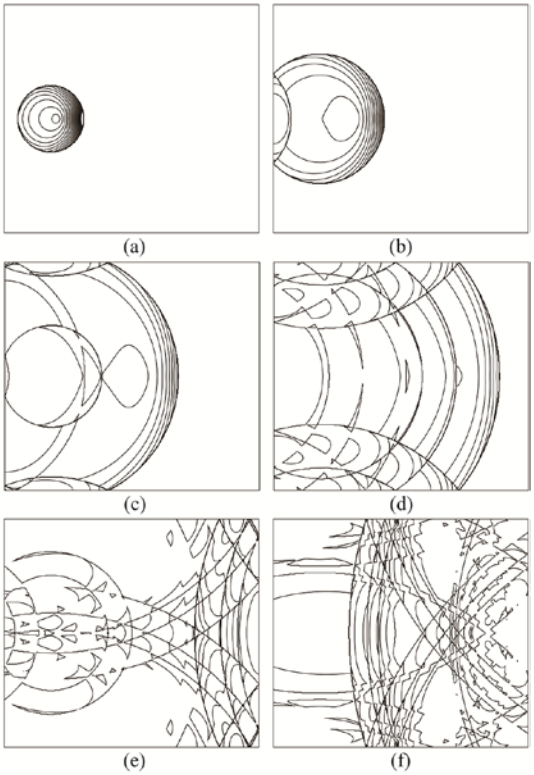

Figure 9. Progressive motion of blast waves in terms of acoustic pressure distributions at a height of 1.2 m inside the space and at certain numerical steps: (a) 100, (b) 250, (c) 550, (d) 800, (e) 1250, and (f) 1800.

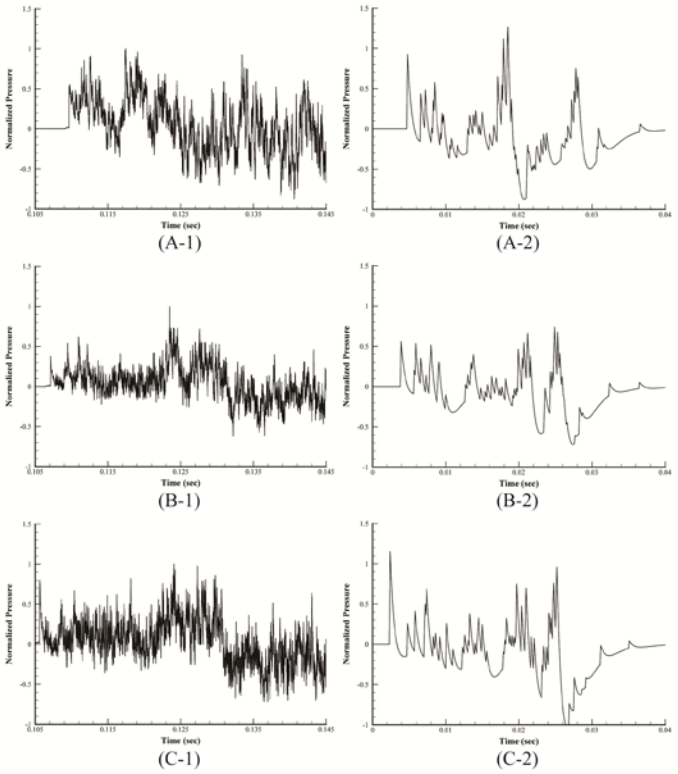

Figure 10. Comparison of measured (left column) and predicted (right column) acoustic pressure signals, which were normalized by the maximum acoustic pressure values measured at the position of each microphone [(A), (B), and (C) in Fig. 8].

location. Furthermore, the geometric divergence and atmospheric absorption, which are considered to be significant attenuation terms during propagation outdoors[25], were imposed as linear effects and could be ignored. Under these conditions, the results shown in Figs. 9 and 10 were obtained using the alternative image theory and discrete wavefront method.

Figure 9 shows the acoustic pressure distributions estimated at a height of 1.2 m inside the space and at certain numerical steps (a) 100, (b) 250, (c) 550, (d) 800, (e) 1250, and (f) 1800. As expected, the blast waves propagated radially into space and were reflected when they arrived at the boundaries. In particular, the waves reflected by the floor and the ceiling were captured very well.

Figure 10 compares the acoustic pressure signals predicted in this study with those measured at the positions of microphones (A), (B), and (C) in Fig. 8. They were normalized by the maximum value of the measured acoustic pressure at each measurement position. To verify the accuracy and validity of the prediction model, first, from a qualitative point of view, the locations of shock fronts observed in the predicted signals were compared with the measured ones. The predicted results cannot be said to agree with the measured signals because the effect of turbulent jet noise was not considered. Nevertheless, the locations of wavefronts corresponding to the shock waves reflected by the enclosing surfaces coincide moderately well with those in the measured results. Thus, the alternative theory and the discrete wavefront method can simulate the propagation of reflected waves inside an enclosed space. Needless to say, there are obviously significant quantitative differences that cannot be ignored. In particular, the rarefactions observed in all of the predicted signals seem to be overestimated. This discrepancy seems to originate in the blast wave model used in the analysis (Fig. 4). Because the waveform agrees well regarding the peak of the positive phase duration but not that of the negative phase duration, overestimated rarefaction might be predicted when the negative phase converged at a certain point. Furthermore, other assumptions imposed in this study, such as a homogeneous atmosphere (i.e., a constant speed of sound and linear geometric divergence effect), might affect the predicted results. In addition, the directivity pattern adopted from the least square method could contribute to contamination of the numerical results.

IV. Concluding Remarks

In the present study, the propagation of blast waves inside an enclosed space was simulated by the alternative image theory and discrete wavefront method. In particular, it is remarkable that its validity and ability to investigate the propagation of blast waves, which are representative of nonlinear phenomena, were verified using a simple and efficient method. The numerical results of these methods also suggest their potential. Although the effects of the surface boundary and nonlinearities received little attention in this research, they will be considered in future works, which is expected to increase the accuracy of the prediction model.

Acknowledgments

This work was supported by the Human Resources Development program (No.20124030200030) of the Korea Institute of Energy Technology Evaluation and Planning (KETEP) grant funded by the Korea government Ministry of Trade, Industry and Energy. In addition, this research was also supported by Basic Science Research Program through the National Research Foundation of Korea (NRF) funded by the Ministry of Education, Science and Technology (No.20120002228).

References

[1]Hirsch, F. G., "Effects of Overpressure on the Ear – A Review," *Annals of the New York Academy of Science*, Vol. 152, No. 1, Oct. 1968, pp. 147-162.

[2]Altmann, J. "Acoustic Weapons – A Prospective Assessment," *Science and Global Security: The Technical Basis for Arms Control, Disarmament, and Nonproliferation Initiatives*, Vol. 9, No. 3, 2001, pp. 165-234.

[3]Branco, N. A. A. C, "Low Frequency Noise: A Major Risk Factor in Military Operations," RTO AVT Symposium on Ageing Mechnisoms and Control: Part A – Developments in Computational Aero- and Hydro-Acoustics, RTO-MP-079(I), Research and Technology Organisation, Neuilly-Sur-Seine Cedex, France, 2003.

[4]Price, G. R. "Firing Recoilless Weapons from Enclosures," U.S. Army Human Engineering Laboratory, Technical Memorandum 20-91, Aberdeen Proving Ground, MD, Oct. 1991.

[5]Ward, W. D. (Editor), "Proposed Damage-Risk Criterion for Impulse Noise (Gunfire)," Rept. of Working Group 57, NAS-NRC Committee on Hearing, Bioacoustics, and Biomechanics, Aug. 1968.

[6]Department of Defense, "Design Criteria Standard – Noise Limits," MIL-STD-1474D, U.S. Army Missile Command, Feb. 1997.

[7]Pfander, F., Bongartz, H., Brinkmann, H., and Kietz, H., "Danger of Auditory Impairment from Impulse Noise: A Comparative Study of the CHABA Damage-Risk Criteria and those of the Federal Republic of Germany," *Journal of Acoustical Society of America*, Vol. 67, No. 2, Feb. 1980, pp. 628-633.

[8]Chan, P. C., Kevin, H. H., Kan, K. K., Stuhmiller, J. H., and Mayorga, M. A., "Evaluation of Impulse Noise Criteria using Human Volunteer Data," *Journal of Acoustical Society of America*, Vol. 110, No. 4, Oct. 2001, pp. 1967-1975.

[9]Drullman, R. (Editor), "Reconsideration of the Effects of Impulse Noise," RTO Human Factors and Medicine Panel, RTO Technical Report TR-017, Research and Technology Organization, Apr. 2003.

[10]Murphy, W. J. and Kardous, C. A., "A Case for using A-weighted Equivalent Energy as a Damage Risk Criterion," Division of Applied Research and Technology, Engineering and Physical Hazard Branch, EPHB Report No. 350-11a, National Institute for Occupational Safety and Health, Jan. 2012.

[11]Dancer, A. and Franke, R., "Hearing Hazard from Impulse Noise: A Comparative Study of Two Clasical Criteria for Weapon Noises (Pfander Criterion and Smoorenburg Criterion) and the LAeq8 Method," *Acta Acustica*, Vol. 3, 1995, pp. 539-547.

[12]Desarnaulds, V., Monay, G., and Favarger, D., "Shooting Noise Regulation – Review of Various National Practices," Proceedings of Internoise 98, I-INCE, 1998.

[13]Garinther, G. R. and Hodge, D. C., "Small-Rocket Noise: Hazards to Hearing (Advanced LAW Program)," U.S. Army Human Engineering Laboratories, Technical Memorandum 7-71, Aberdeen Research and Development Center, Aberdeen Proving Ground, MD, May 1971.

[14]Price, G. R., "Firing from Enclosures with 90 mm Recoilless Rifle: Assessment of Acoustic Hazard," U.S. Army Human Engineering Laboratory, Technical Memorandum 11-78, Aberdeen Proving Ground, MD, May 1978.

[15]Patterson Jr., J. H., "Proposed New Procedure for Estimating Allowable Number of Rounds for Blast Overpressure Hazard Assessment," U.S. Army Aeromedical Research Laboratory, USAARL Report No. 98-03, Fort Rucker, AL, Nov. 1997.

[16]Jokel, C. and Patterson, J. H, "Criteria and Procedures for Auditory Health Hazard Assessment of Impulse Noise (Blast Over Pressure)," U.S. Army Public Health Command, Technical Guide No. 338, Feb. 2012.

[17]Kong, B., Lee, K., and Lee, S., "An Alternative Image Theory for Indoor Sound Propagation," Proceedings of Internoise 2012, I-INCE, New York, 2012.

[18]Attenborough, K., "Sound Propagation in the Atmosphere," Handbook of Acoustics, edited by T. D. Rossing, Springer Science+Business Media, New York, 2007, pp. 113-147.

[19]Kinsler, L. E., Frey, A. R., Coppens, A. B., and Sanders, J. V., *Fundamentals of Acoustics*, 4th ed., John Wiley and Sons, New York, Chaps. 17, 2000.

[20]Friedlander, F. G., "The diffraction of Sound Pulses. I. Diffraction by a Semi-Infinite Plane," Proceedings of the Royal Society of London. Series A, Mathematical and Physical Sciences, Vol. 186, No. 1006, Sep. 1946, pp. 322-344.
[21]Morfey, C. L, *Dictionary of Acoustics*, Academic Press, London, 2001.
[22]Pierce, A.D., *Acoustics: An Introduction to Its Physical Principles and Applications*, 1989 ed, Acoustical Society of America, New York, 1991.
[23]Tam, C. K. W., *Computational Aeroacoustics – A Wave Number Approach*, Cambridge University Press, New York, 2012.
[24]Tam, C. K. W. and Webb, J. C., "Dispersion-Relation-Preserving Finite Difference Schemes for Computational Acoustics," *Journal of Computational Physics*, Vol. 107, 1993, pp. 262-281.
[25]ISO 9613-2:1996(E), "Acoustics – Attenuation of Sound during Propagation Outdoors – Part 2: General Method of Calculation," International Organization for Standardization, Geneva, Switzerland, 2003.